Transverse magnetic field effects on metastable states of magnetic island chains

G. M. Wysin*
Department of Physics, Kansas State University, Manhattan, KS 66506-2601
(Dated: October 3, 2024)

A one-dimensional chain of elongated anisotropic magnetic islands on a nonmagnetic substrate with dipolar interactions and an applied magnetic field transverse to the chain is considered. With the long axes of the islands perpendicular to the chain, the system allows for three uniform metastable states: (1) tilted dipoles with magnetization at an oblique angle to the chain, (2) transverse dipoles with magnetization perpendicular to the chain, and (3) alternating transverse dipoles with no net magnetization. The uniform magnetic field controls their stabilities and is analyzed for its ability to cause transitions among the states. The energy and frequency eigenvalues are determined for small-amplitude traveling wave deviations of the dipoles. The results are summarized in a phase diagram in the field/anisotropy plane, that highlights the multistable properties of this type of system.

PACS numbers: 75.75.+a, 85.70.Ay, 75.10.Hk, 75.40.Mg
Keywords: magnetics, magnetic islands, frustration, dipole interactions, metastability, magnon modes.

I. ONE-DIMENSIONAL CHAINS OF THIN MAGNETIC ISLANDS

Arrays of elongated magnetic nanoislands fabricated on nonmagnetic substrates, such as two-dimensional (2D) artificial spin ices (ASI) [1, 2] and one-dimensional (1D) dipolar chains [3, 4] have many interesting features, depending on the geometry and competition between shape anisotropy and dipolar interactions. In a leading approximation for high aspect ratio islands, their dipole moments are usually approximated as Ising-like [5], as shape anisotropy makes them preferentially point close to the long axes of the islands (Ref. [6], Ch. 3). 2D artificial spin ices exhibit geometrical frustration [7], wherein even the lowest energy states cannot find a configuration that simultaneously minimizes all of the interaction energies. For square lattice ASI, the ground state possesses antiferromagnetic order, as nearest neighbor dipoles alternate in direction while trying (but failing) to simultaneously minimize the anisotropy energy and dipolar energy.

A strong applied field that is slowly turned off can leave 2D ASI in a higher energy metastable remanent state, that possesses nonzero magnetization, while being locally stable against small perturbations that do not cause a direct transition back to the ground state. There has been substantial interest in finding the differences in the magnetic oscillation modes in ground and excited states of ASI [8–10], mostly through numerical simulations. A simplified model was solved analytically for the modes in square lattice ASI in the ground state [11] and for remanent states [12], assuming Heisenberg-like dipoles with three spin components [13, 14], all without the effects of an applied magnetic field. The motivation is that different dipolar configurations should be characterized by their dynamic modes [15, 16]. Further, physical modification of the system by pressure or stress might be useful for modifying its dynamic properties [17]. The mode spectrum also implies the conditions needed for instability of a chosen dipolar configuration, and this information can be used to predict transitions of the system from an unstable state to a stable state.

A 1D chain of islands whose long axes are perpendicular to the chain has been studied [18] for some of its similarities to 2D ASI, and this article concerns its properties when a magnetic field $\mathbf{B}$ is applied perpendicular to the chain. The system is depicted in Fig. 1, where x is along the chain, y is transverse, and z is perpendicular to the substrate. It is assumed that the islands are thin perpendicular to the substrate, and only weakly elongated, leading to easy-plane anisotropy in the substrate combined with moderate easy-axis anisotropy along the longer axes [19]. Assuming single-domain magnetic structure in each nano-sized island, their net dipole moments are Heisenberg-like, and their dynamics can be analyzed using Hamiltonian spin dynamics [20] (no Ising approximation). For $\mathbf{B} = 0$, the model allows for two states with remanent magnetization, either parallel to the chain (called x-parallel) or perpendicular to the chain (called y-parallel), and one with the dipoles alternately pointing perpendicular to the chain (called y-alternating). The x-parallel and y-parallel states resemble remanent states of ASI, and the y-alternating state is reminiscent of the alternating ground state of square ASI.

The small-amplitude magnetic oscillations were determined for each type of state in Ref. [18], *without* a magnetic field, as functions of the anisotropy and dipolar strengths. The anisotropy relative to dipolar interaction needed to stabilize each type of state was determined. It was found that x-parallel and y-alternating states destabilize one into the other with a fluctuation at wavevector $q = \pi/a$, where a is the island spacing. In contrast, the metastable y-parallel state destabilizes into y-alternating

*Electronic address: wysin@k-state.edu; URL: http://www.phys.ksu.edu/personal/wysin

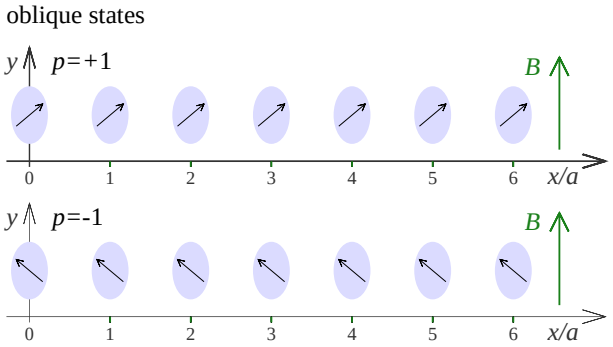

FIG. 1: The two possible oblique states, distinguished by dipoles with positive x-components ($p = +1$) or negative x-components ($p = -1$). With increasing applied field B, the dipolar energy per site changes from $-2\zeta_R D$ at $B = 0$ (dipoles in $\pm x$ directions) to $+\zeta_R D$ at $\mu B_{\max} = 2(3\zeta_R D - K_1)$ (dipoles parallel to B).

with a fluctuation at wavevector $q = 0$ (but not *vice-versa*). Surprisingly, that transition takes place at an easy-axis anisotropy value where y-parallel has the same energy as x-parallel, even though x-parallel is absolutely unstable there, see Fig. 9 of Ref. [18].

A uniform magnetic field $\mathbf{B}$ applied transverse to the chain direction has significant consequences. To start with, the dipoles in an x-parallel state are tilted in the field direction away from the chain direction, as in Fig. 1, hence they are renamed as *oblique* states now. Especially, this study shows how an applied field can switch the system among the three states mentioned. Additionally, the results indicate how it is dynamic fluctuations that determine metastability, which is not directly connected to energy differences among the states, as might have been naïvely assumed.

After finding the new static states when the field is applied, the small-amplitude oscillations about each state will be determined using undamped Heisenberg spin dynamics. Based on those spectra, the anisotropy and field strengths at which each state is locally stable (*i.e.*, metastable) or unstable will be determined. The results for all three states taken together will be used to describe possibilities for transitions among them.

General features of the states found here could be measurable with magnetic force microscopy [21] or magneto-optic techniques [22, 23] in similar 1D systems, such as chains of biomineralized magnetosomes [24], patterned Permalloy elements [25], Fe nanoparticles [26], Co_2C nanoparticles [27], and nanowire elements [28]. The results will imply particular jumps or other features in the magnetization plotted versus applied field, although the emphasis of this study is on the states' stability as a function of anisotropy and field.

II. THE HEISENBERG-LIKE MACRO-DIPOLE MODEL

For single-domain magnetic islands (small enough with strong internal ferromagnetic exchange), the state of one island can be approximated as a single magnetic dipole of fixed magnitude μ, and arbitrary direction [20]. A particular dipole is denoted $\mu\mathbf{S}_n$, where $\mathbf{S}_n$ is a unit spin vector. It will be convenient to write these spin vectors using planar spherical angles (ϕ_n, θ_n), where ϕ_n is an azimuthal angle in the xy-plane and θ_n is the tilting of a spin out of the xy-plane, i.e.,

$$\begin{aligned}\mathbf{S}_n &= (S_n^x, S_n^y, S_n^z) \\ &= (\cos\theta_n \cos\phi_n, \cos\theta_n \sin\phi_n, \sin\theta_n). \end{aligned} \tag{1}$$

For dynamics, S_n^z is the momentum conjugate to ϕ_n.

The islands are assumed to have moderately strong shape anisotropies that tend to cause their net dipole moment to point within the plane of the island (xy) and prefer to point along its long axis (y-direction). These preferences are represented mathematically through an easy-plane anisotropy $K_3 > 0$ and an easy-axis anisotropy $K_1 > 0$, see [19]. The n^{th} island's anisotropy contribution to the Hamiltonian is expressed alternatively in Cartesian or spherical coordinates as

$$\begin{aligned}H_n^K &\equiv -K_1 \left(S_n^y\right)^2 + K_3 \left(S_n^z\right)^2 \\ &= -K_1 \cos^2\theta_n \sin^2\phi_n + K_3 \sin^2\theta_n. \end{aligned} \tag{2}$$

Each island interacts with the applied field transverse to the chain, whose contribution to the Hamiltonian is

$$H_n^B = -\mu B S_n^y = -\mu B \cos\theta_n \sin\phi_n. \tag{3}$$

The chain itself is along the x direction, with nearest-neighbor (NN) pair separation at lattice constant a. Pairs of dipoles interact via long-range dipolar interactions. With μ_0 being the permeability of vacuum, define the energy constant for dipolar interaction of NN-pairs,

$$D = \frac{\mu_0 \mu^2}{4\pi a^3}. \tag{4}$$

D will be used as the fundamental energy scale in this work. The dipole interaction is reduced relative to this by the cube of the separation distance r measured in lattice constants, which is an integer, $k = r/a$. With unit vector $\hat{x}$ along the chain direction, the dipolar pair interaction between island n and island $n + k$ is

$$\begin{aligned}H_{n,k}^D &\equiv \frac{D}{k^3}\left[\mathbf{S}_n \cdot \mathbf{S}_{n+k} - 3(\mathbf{S}_n \cdot \hat{x})(\mathbf{S}_{n+k} \cdot \hat{x})\right] \\ &= \frac{D}{k^3}\big[\sin\theta_n \sin\theta_{n+k} + \cos\theta_n \cos\theta_{n+k} \\ &\quad \times (-2\cos\phi_n \cos\phi_{n+k} + \sin\phi_n \sin\phi_{n+k})\big]. \end{aligned} \tag{5}$$

Then the Hamiltonian for a chain of N dipoles exposed to a uniform magnetic field of strength B along the y-direction is taken as

$$H = \sum_{n=1}^{N} \left(H_n^K + H_n^B + \sum_{k=1}^{R} H_{n,k}^D \right). \tag{6}$$

An upper limit R is used on the range of the dipolar interactions. When $R = 1$, it reverts to a NN-model. By summing over all n, and only positive values of separation k, each dipole-dipole pair interaction is included once. To avoid end effects, it will generally be assumed that $N \to \infty$ and per-site energies will be most relevant. The model calculated with infinite range dipole interactions ($R \to \infty$) will be referred to as the long-range dipole (LRD) model. In a 1D model, convergence of the needed sums is fairly rapid. Results for the LRD model are different from that for NN interactions only by a slight rescaling of energy and frequency eigenvalues, as well as a slight rescaling of the stable state phase diagram obtained later.

III. FINDING STATIONARY STATES WITH APPLIED FIELD PRESENT

Initially, uniform stationary states where the dipoles are all parallel are considered. The field will tend to tilt the dipoles away from the chain direction. Therefore we take all of the spin's angles to be the same unknown values, (ϕ, θ). The Hamiltonian per site $u = H/N$ becomes

$$u = \sum_{k=1}^{R} \frac{D}{k^3}\left(1 - 3\cos^2\theta\cos^2\phi\right) - K_1\cos^2\theta\sin^2\phi + K_3\sin^2\theta - \mu B\cos\theta\sin\phi. \quad (7)$$

A possible state should minimize this energy. The derivatives with respect to θ and ϕ must be zero:

$$\frac{\partial u}{\partial\theta} = \left[6\zeta_R D\cos^2\phi + 2K_1\sin^2\phi + 2K_3\cos\theta + \mu B\sin\phi\right]\sin\theta = 0, \quad (8)$$

$$\frac{\partial u}{\partial\phi} = \left[(6\zeta_R D - 2K_1)\cos\theta\sin\phi - \mu B\right]\cos\theta\cos\phi = 0. \quad (9)$$

The dipole sum over range $R \geq 1$ is defined as

$$\zeta_R \equiv \sum_{k=1}^{R}\frac{1}{k^3}. \quad (10)$$

For infinite range interactions, this becomes a zeta function, $\zeta_\infty = \zeta(3) \approx 1.2020569$, while the value for the NN model is simply $\zeta_1 = 1$.

A. Oblique states for $B \neq 0$

Solving Eqs. (8) and (9), (0) superscripts are used to indicate values that minimize the per-site energy, u. The first solution from Eq. (8) has $\theta^{(0)} = 0$, but $S_n^y = \sin\phi^{(0)}$ takes on a value from Eq. (9) that increases with the applied field, satisfying

$$1 \geq S_n^y = \sin\phi^{(0)} = \frac{\mu B/2}{3\zeta_R D - K_1} \geq 0. \quad (11)$$

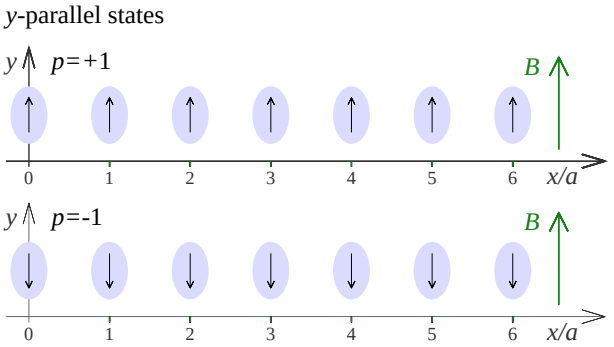

FIG. 2: The two possible y-parallel states, with dipoles uniformly aligned ($p = +1$) or anti-aligned ($p = -1$) with the applied field. The field causes an energy difference between them.

For $B \to 0$, the dipoles are parallel to the chain direction ($\phi^{(0)} = 0, \pi$), which are the x-parallel states formerly discussed [18]. A nonzero applied field tilts the dipoles uniformly towards the field direction, as in Fig. 1, now referred to as *oblique* states. There are two oblique states: one with positive x-components of the dipoles (a *polarization* along x of $p = +1$) and one with negative x-components (polarization $p = -1$). The dipoles have the same y-components in both oblique states.

With or without an applied field, the magnetization is saturated, and the field works to rotate it away from the chain direction. In the case of zero applied field, the dipolar energy is minimized while the K_1 anisotropy energy is maximized. A nonzero field brings these energies into competition. The per-site energy for oblique states is found to be

$$u_{\rm oblq} = -2\zeta_R D - \frac{(\mu B/2)^2}{3\zeta_R D - K_1}. \quad (12)$$

The field lowers the energy of both oblique states equally.

Based on the factor in the denominator of Eq. (11), an oblique state can only exist for $K_1 < 3\zeta_R D$. In the absence of a field for the NN-model, stability has been shown to require $K_1 < D$. Although a complete stability analysis is presented below, this indicates that the applied field is able to extend the range of stability of x-parallel states by tilting the dipoles, forming an oblique state, and lowering the energy. This suggests that under appropriate conditions, an oblique state created while a field is applied could be destroyed or transformed to another state by turning off the field.

B. y-parallel or transverse states

A second solution obtained from Eqs. (8) and (9) has uniform angles

$$\theta^{(0)} = 0, \quad \phi^{(0)} = p\frac{\pi}{2}, \quad (13)$$

where its polarization along y is $p = \pm 1$. The nonzero spin components are

$$S_n^y = p = \pm 1. \tag{14}$$

The dipoles point perpendicular to the chain direction, either parallel ($p = +1$) or antiparallel ($p = -1$) to the applied field $\mathbf{B}$, see Fig. 2. These are states with a saturated transverse magnetization, called y-parallel states in an earlier report or y-par for short. The y-parallel states minimize the anisotropy energy but not the dipolar energy. It is clear that the state polarized parallel to $\mathbf{B}$ should exhibit greater stability (it minimizes the applied field energy), and conversely, the antiparallel state will become unstable once the field surpasses some maximum. The per-site energy is found to be

$$u_{y\text{-par}} = \zeta_R D - K_1 - p\mu B. \tag{15}$$

While the y-parallel states take the same perpendicular structure, regardless of the field, their stability is indeed influenced by the field, which is analyzed below.

C. y-alternating states

A third type of stationary state is possible, primarily due to NN dipolar interactions, where the dipoles alternate by site, pointing in $\pm y$-directions perpendicular to the chain, called y-alternating or y-alt for short. The structure will produce a dipolar energy that is less than that in a y-parallel state, but not as low as in oblique states.

To analyze this configuration, two sublattices A and B are assumed. Let the A sublattice be the n=even sites and the B sublattice be the n=odd sites, and assume spin angles (ϕ_A, θ_A) and (ϕ_B, θ_B), uniform by sublattice. Start with nearest-neighbor dipole interactions only. Each dipolar interaction is between A and B sites, at distance $r = a$ or $k = 1$.

Averaging over A and B sites, the per-site energy is

$$\begin{aligned} u =& D\big[\cos\theta_A\cos\theta_B\cos(\phi_A-\phi_B) + \sin\theta_A\sin\theta_B - 3\cos\theta_A\cos\theta_B\cos\phi_A\cos\phi_B\big] \\ & - \frac{K_1}{2}(\cos^2\theta_A\sin^2\phi_A + \cos^2\theta_B\sin^2\phi_B) + K_3(\sin^2\theta_A + \sin^2\theta_B) - \frac{\mu B}{2}(\cos\theta_A\sin\phi_A + \cos\theta_B\sin\phi_B). \end{aligned} \tag{16}$$

This is now minimized with respect to the four angles. A brief calculation shows that

$$\frac{\partial u}{\partial\theta_A} = \frac{\partial u}{\partial\theta_B} = 0 \tag{17}$$

is satisfied by

$$\theta_A^{(0)} = \theta_B^{(0)} = 0. \tag{18}$$

Statically, the spins remain in the xy-plane. The remaining equations are of this form:

$$\begin{aligned} \frac{\partial u}{\partial\phi_A} =& D\big[-\sin(\phi_A-\phi_B) + 3\sin\phi_A\cos\phi_B\big] \\ & - K_1\sin\phi_A\cos\phi_A - \frac{\mu B}{2}\cos\phi_A = 0. \end{aligned} \tag{19}$$

Letting $\phi_B = \phi_A$ recovers the oblique and y-parallel states. Instead, trying $\phi_B = -\phi_A$ produces

$$\big[(D - K_1)\sin\phi_A - \tfrac{1}{2}\mu B\big]\cos\phi_A = 0, \tag{20}$$

and this is solved by

$$\phi_A^{(0)} = p\frac{\pi}{2} = -\phi_B^{(0)}, \quad p = \pm 1. \tag{21}$$

There are two degenerate solutions corresponding to the two choices of p. The alternating angles correspond to dipoles alternating in direction by site,

$$S_n^y = (-1)^n p. \tag{22}$$

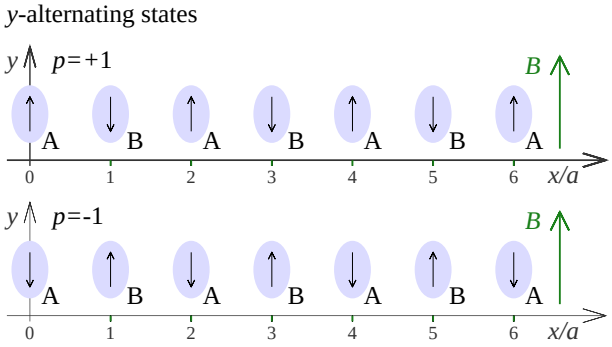

FIG. 3: The two possible y-alternating states, with dipoles at even sites aligned ($p = +1$) or anti-aligned ($p = -1$) with the applied field, and dipoles at odd sites in the opposing direction. The field does not influence the state energy but does affect the stability.

The two possible y-alt states are shown in Fig. 3. While they exhibit antiferromagnetic order, the interaction is dipolar and the structure has nothing to do with antiferromagnetism. Hence the preferred name is y-alternating or just y-alt.

One can assume the same alternating structure might exist even with longer range dipole interactions, and later investigate its stability. Consider the energy per

site. The dipolar contributions around a central A-site alternate in sign, as they change between AB bonds ($\phi_A - \phi_B = p\pi$) and AA bonds ($\phi_A - \phi_A = 0$). Thus, the energy per site for y-alternating states is seen to be

$$u_{y\text{-alt}} = D\sum_{k=1}^{R}\frac{(-1)^k}{k^3} - K_1. \tag{23}$$

The sum needed here can be expressed by separating even and odd contributions, which involve

$$\begin{aligned} s_{\rm e} &= \sum_{k=2,4,6\ldots}^{R}\frac{1}{k^3} = \tfrac{1}{8}\sum_{k=1}^{R}\frac{1}{k^3} = \tfrac{1}{8}\zeta_R, \\ s_{\rm o} &= \sum_{k=1,3,5\ldots}^{R}\frac{1}{k^3} = \sum_{k=1}^{R}\frac{1}{k^3} - \sum_{k=2,4,6\ldots}^{R}\frac{1}{k^3} = \tfrac{7}{8}\zeta_R. \end{aligned} \tag{24}$$

Then the sum needed is

$$\sum_{k=1}^{R}\frac{(-1)^k}{k^3} = -\tfrac{7}{8}\zeta_R + \tfrac{1}{8}\zeta_R = -\tfrac{3}{4}\zeta_R, \tag{25}$$

and the y-alt state energy per site is independent of p and the applied field,

$$u_{y\text{-alt}} = -\tfrac{3}{4}\zeta_R D - K_1. \tag{26}$$

Even though B is absent in this expression, the field strength determines the stability of y-alt states.

IV. DYNAMICS AND STABILITY

Suppose there is a gyromagnetic ratio $\gamma_{\rm e}$ that converts angular momenta $\mathbf{L}_n$ into magnetic dipole moments via $\vec{\mu}_n = \gamma_{\rm e}\mathbf{L}_n$. Then the undamped free dynamics of a magnetic dipole system follows a torque equation for the time derivative of $\mathbf{L}_n$ (see Ref. [6], Ch. 5),

$$\frac{d\mathbf{L}_n}{dt} = \vec{\tau}_n = \vec{\mu}_n \times \mathbf{B}_n^{\rm eff}, \tag{27}$$

where the Hamiltonian involves effective fields $\mathbf{B}_n^{\rm eff}$ at each site, $H = -\sum_n \vec{\mu}_n \cdot \mathbf{B}_n^{\rm eff}$. This gives

$$\frac{1}{\gamma_{\rm e}}\frac{d\vec{\mu}_n}{dt} = \vec{\mu}_n \times \left(-\frac{\partial H}{\partial \vec{\mu}_n}\right). \tag{28}$$

Transforming the dipoles to the spherical coordinates in (1), the mechanics is that where ϕ_n are generalized coordinates and $\sin\theta_n$ are the corresponding conjugate momenta. The dynamics obeys Hamiltonian equations,

$$\begin{aligned} \frac{\mu}{\gamma_{\rm e}}\frac{d}{dt}\phi_n &= \frac{\partial H}{\partial \sin\theta_n}, \\ \frac{\mu}{\gamma_{\rm e}}\frac{d}{dt}\sin\theta_n &= -\frac{\partial H}{\partial \phi_n}. \end{aligned} \tag{29}$$

A. Linearization of H

In practice, we consider the dynamics linearized around the three types of states described above, all of which have $\theta^{(0)} = 0$. At each site of the chain, let the in-plane angle be replaced as $\phi_n \to \phi^{(0)} + \phi_n$, where $\phi_n \ll 1$ now represents a small deviation from the equilibrium value. Similarly, with $\theta^{(0)} = 0$, use $\theta_n \ll 1$ to represent a small deviation from zero. Then the Hamiltonian is expanded to quadratic orders in these deviations, and from there the linearized dynamics and stability can be determined.

The sets of in-plane and out-of-plane deviations can be represented by row vectors of the ϕ_n and θ_n angles,

$$\psi_\phi^\dagger = (\phi_1, \phi_2, \phi_3 \ldots), \quad \psi_\theta^\dagger = (\theta_1, \theta_2, \theta_3 \ldots). \tag{30}$$

The Hamiltonian is expanded in terms of these as

$$H = H^{(0)} + H^{(1)} + H^{(2)}. \tag{31}$$

$H^{(0)}$ is the minimized state energy that does not depend on the deviations ϕ_n, θ_n. $H^{(1)}$ is the terms linear in ϕ_n and θ_n, which is zero because the state is an energy minimum. $H^{(2)}$ is the deviation energy, a double quadratic form in the deviations,

$$\begin{aligned} H^{(2)} &= H_\phi + H_\theta, \\ H_\phi &= \psi_\phi^\dagger \boldsymbol{M}_\phi \psi_\phi, \quad H_\theta = \psi_\theta^\dagger \boldsymbol{M}_\theta \psi_\theta. \end{aligned} \tag{32}$$

The elements of the matrices $\boldsymbol{M}_\phi$ and $\boldsymbol{M}_\theta$ come from expanding around each of the three states. These matrices determine the traveling wave fluctuations of the system, and instabilities of those waves (such as imaginary eigenfrequencies) signal instability of a state.

B. Linearized dynamics, energy eigenvalues, instabilities

With the Hamiltonian linearized and described by matrices $\boldsymbol{M}_\phi$ and $\boldsymbol{M}_\theta$, even including long-range dipole interactions, the dynamic equations of motion (29) take the form,

$$\begin{aligned} \frac{\mu}{\gamma_{\rm e}}\dot{\phi}_n &= +2\sum_{k=-R}^{+R} M_{\theta,n,n+k}\theta_{n+k}, \\ \frac{\mu}{\gamma_{\rm e}}\dot{\theta}_n &= -2\sum_{k=-R}^{+R} M_{\phi,n,n+k}\phi_{n+k}, \end{aligned} \tag{33}$$

where dot signifies time derivative. The sums include diagonal or on-site matrix elements ($k = 0$) as well as dipole pair interactions at separations $k \neq 0$ out to range R in both directions. This is equivalent to the pair of matrix equations,

$$\frac{\mu}{\gamma_{\rm e}}\dot{\psi}_\phi = +2\boldsymbol{M}_\theta\psi_\theta, \qquad \frac{\mu}{\gamma_{\rm e}}\dot{\psi}_\theta = -2\boldsymbol{M}_\phi\psi_\phi, \tag{34}$$

where ψ_ϕ and ψ_θ are column vectors of the angles. In a system with a single sublattice, these equations allow for travelling waves with small amplitudes a_ϕ and a_θ and frequency ω,

$$\phi_n = a_\phi e^{\mathrm{i}(qna-\omega t)}, \qquad \theta_n = a_\theta e^{\mathrm{i}(qna-\omega t)}. \tag{35}$$

where the allowed wavevectors for periodic boundary conditions are

$$q \equiv \frac{2\pi m}{Na}, \quad m = 0, 1, 2...(N-1). \tag{36}$$

The equations of motion (33) condense into a pair of equations involving only the two amplitudes,

$$\begin{aligned} -\mathrm{i}\omega a_\phi &= +2\frac{\gamma_\mathrm{e}}{\mu}\lambda_\theta a_\theta, \\ -\mathrm{i}\omega a_\theta &= -2\frac{\gamma_\mathrm{e}}{\mu}\lambda_\phi a_\phi. \end{aligned} \tag{37}$$

These are expressed in terms of energy eigenvalues λ_ϕ and λ_θ of the $\boldsymbol{M}_\phi$ and $\boldsymbol{M}_\theta$ matrices, defined in a usual way,

$$\boldsymbol{M}_\phi \psi_\phi = \lambda_\phi \psi_\phi, \quad \boldsymbol{M}_\theta \psi_\theta = \lambda_\theta \psi_\theta, \tag{38}$$

where ψ_ϕ and ψ_θ are column eigenvectors composed from the site angles. Therefore, the frequency for a travelling wave at wavevector q is

$$\omega(q) = 2\frac{\gamma_\mathrm{e}}{\mu}\sqrt{\lambda_\phi \lambda_\theta}. \tag{39}$$

Results are given for frequencies in terms of a frequency unit based on the NN-dipolar coupling frequency,

$$\delta_1 \equiv \frac{\gamma_\mathrm{e} D}{\mu}, \tag{40}$$

as in Fig. 4 and the other $\omega(q)$ dispersion relation plots.

Assuming inversion symmetry, the eigenvalue problems can be written in a form,

$$M_{\phi,n,n}\phi_n + \sum_{k=1}^{R} M_{\phi,n,n+k}(\phi_{n+k} + \phi_{n-k}) = \lambda_\phi \phi_n. \tag{41}$$

Then the energy eigenvalues obtained for the assumed travelling waves can be expressed as

$$\begin{aligned} \lambda_\phi(q) &= M_{\phi,n,n} + 2\sum_{k=1}^{R} M_{\phi,n,n+k}\cos kqa, \\ \lambda_\theta(q) &= M_{\theta,n,n} + 2\sum_{k=1}^{R} M_{\theta,n,n+k}\cos kqa. \end{aligned} \tag{42}$$

The expressions apply to the translationally invariant oblique and y-parallel states. For the y-alternating states, a similar procedure but with a two-sublattice wave assumption is applied in Sec. IV E.

Instabilities of a given state will be considered due to varying the anisotropy constants or the applied field. An instability is associated with an arbitrary fluctuation that lowers the energy. That is indicated when one of the energy eigenvalues λ_ϕ or λ_θ becomes zero or even negative at some wavevector. If either eigenvalue goes to zero or becomes negative, then the frequency $\omega(q)$ also goes to zero or becomes imaginary.

This method determines the presence of any dynamic instability in the chosen state. Further, the wavevector where that occurs gives an indication of the unstable change in structure of the state, and hence is a guide towards what structure will result if the instability takes over the dynamics. These properties are determined separately for oblique, y-parallel and y-alternating states, after determining their dynamic matrices $\boldsymbol{M}_\phi$ and $\boldsymbol{M}_\theta$.

C. Linearized analysis of oblique states

For oblique states, small deviations of the dipoles away from equilibrium are considered. The analysis is complicated by the fact that in equilibrium the dipoles are tilted away from the x-axis when a field is applied along the y-axis. Energy changes are considered when small deviations take place relative to that oblique direction.

1. *Expanding H for oblique states*

For an oblique state, the in-plane angles ϕ_n are replaced by $\phi_n \to \phi^{(0)} + \phi_n$, where $\phi^{(0)}$ is the equilibrium value given in Eq. (11) and ϕ_n is now the *deviation* from that. The out-of-plane deviations are θ_n. To facilitate the algebra, use a notation,

$$s_0 = \sin\phi^{(0)}, \quad c_0 = \cos\phi^{(0)}. \tag{43}$$

Then the expansion of a dipole pair interaction in H for site n interacting with site $n+k$, to quadratic order in deviations, is

$$\begin{aligned} H^D_{n,k} \approx \frac{D}{k^3}\Big[&(c_0^2 - \tfrac{1}{2}s_0^2)(-2 + \phi_n^2 + \phi_{n+k}^2 + \theta_n^2 + \theta_{n+k}^2) \\ &+ (c_0^2 - 2s_0^2)\phi_n\phi_{n+k} + \theta_n\theta_{n+k} + 3c_0 s_0(\phi_n + \phi_{n+k})\Big]. \end{aligned} \tag{44}$$

This is summed over all n but only with $k \geq 1$ to count all pairs. The anisotropy energy at a site is

$$H^K_n \approx -K_1[s_0^2(1 - \phi_n^2 - \theta_n^2) + c_0^2\phi_n^2 + 2c_0 s_0\phi_n] + K_3\theta_n^2. \tag{45}$$

The field term is

$$H^B_n \approx -\mu B\left[s_0(1 - \tfrac{1}{2}\phi_n^2 - \tfrac{1}{2}\theta_n^2) + c_0\phi_n\right]. \tag{46}$$

The combination of all these parts gives the per-site Hamiltonian, and in this case we see zeroth, first, and

quadratic order parts, $H_n \approx H_n^{(0)} + H_n^{(1)} + H_n^{(2)}$. The zeroth is

$$H_n^{(0)} = \left(\sum_{k=1}^{R} \frac{1}{k^3}\right) D(-2c_0^2 + s_0^2) - K_1 s_0^2 - \mu B s_0. \quad (47)$$

Minimized with respect to s_0, the equilibrium results of Eq. (11) for s_0 and $\phi^{(0)}$ are recovered. In first order, there is

$$H_n^{(1)} = \left[\left(\sum_{k=1}^{R} \frac{1}{k^3}\right) 6Ds_0 - 2K_1 s_0 - \mu B\right] c_0 \phi_n. \quad (48)$$

This is identically zero when the equilibrium value of s_0 is inserted, as it should be in a minimizing state. Finally there is the quadratic part,

$$H_n^{(2)} = D\sum_{k=1}^{R} \frac{1}{k^3}[(2-3s_0^2)(\phi_n^2+\theta_n^2) + (1-3s_0^2)\phi_n\phi_{n+k} + \theta_n\theta_{n+k}] - K_1[(c_0^2-s_0^2)\phi_n^2 - s_0^2\theta_n^2] + K_3\theta_n^2 + \tfrac{1}{2}\mu B s_0(\phi_n^2+\theta_n^2). \quad (49)$$

The ϕ and θ contributions are completely decoupled, allowing us to write $H^{(2)} = H_\phi + H_\theta$ and expressing these in the matrix notation of Eq. (32). The elements of matrices $\boldsymbol{M}_\phi$ and $\boldsymbol{M}_\theta$ can be determined, assuming dipole interactions out to maximum range R. Being the coefficients of ϕ_n^2 and θ_n^2 in $H_n^{(2)}$, the on-site elements are surprisingly simple when using the equilibrium value s_0,

$$M_{\phi,n,n} = 2\zeta_R D - K_1 c_0^2, \quad M_{\theta,n,n} = 2\zeta_R D + K_3. \quad (50)$$

The inter-site elements are also simple, being half the coefficients of pairs of angles in $H_n^{(2)}$,

$$M_{\phi,n,n+k} = \frac{D}{2k^3}(1-3s_0^2), \quad M_{\theta,n,n+k} = \frac{D}{2k^3}. \quad (51)$$

Note that the applied field only affects the in-plane parts.

2. *Energy and frequency eigenvalues of oblique states*

The energy eigenvalues associated with small wave-like in-plane deviations (λ_ϕ) and for small wave-like out-of-plane deviations (λ_θ) control the basic dynamics, and as well, determine the states' stability. Using the assumed wave deviation in (35), the eigenvalues of matrices $\boldsymbol{M}_\phi$ and also $\boldsymbol{M}_\theta$ are given by the expression in Eq. (42). Using the matrix elements just found, one has

$$\lambda_\phi(q) = 2\zeta_R D - K_1 c_0^2 + D(1-3s_0^2)\sum_{k=1}^{R} \frac{1}{k^3}\cos kqa,$$
$$\lambda_\theta(q) = 2\zeta_R D + K_3 + D\sum_{k=1}^{R} \frac{1}{k^3}\cos kqa. \quad (52)$$

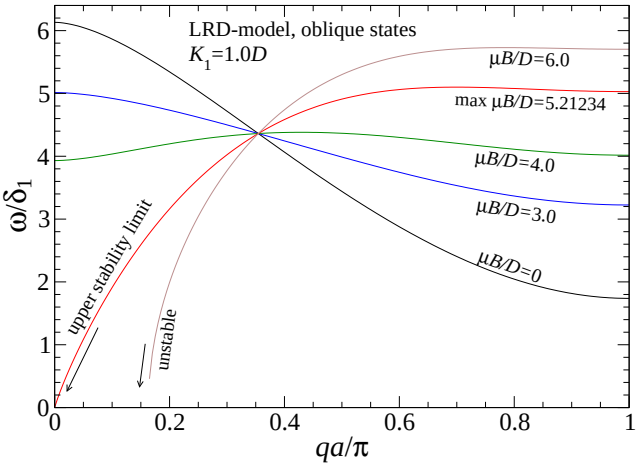

FIG. 4: Mode frequencies from Eq. (39) in the LRD-model for oblique states with $K_1 = 1.0D$, $K_3 = 0$, with a transverse applied field strength as indicated. The frequency unit δ_1 is defined in Eq. (40). At $\mu B_{\max} \approx 5.21234D$, the $q = 0$ frequency becomes zero and that is the limit for stability. For $\mu B > 5.21234D$, imaginary values of ω are present near low q and the state is absolutely unstable.

The sum in each expression is a finite-range Clausen function [29] of order 3,

$$\mathrm{Cl}_{R,3}(qa) = \sum_{k=1}^{R} \frac{\cos kqa}{k^3}. \quad (53)$$

In the limit $R \to \infty$, notable values are

$$\mathrm{Cl}_3(0) = \zeta(3) \approx 1.2020569,$$
$$\mathrm{Cl}_3(\pi) = -\tfrac{3}{4}\zeta(3) \approx -0.901542677\,. \quad (54)$$

Only $\lambda_\phi(q)$ is affected by the applied field.

Frequencies $\omega(q)$ as obtained from (39) are shown in Fig. 4 for $K_1 = 1.0D$, $K_3 = 0$, and a range of applied field values $\mu B/D$ from 0 to 6. This is an anisotropy value that does not require an applied field being present for stability. There is a q-value where all the dispersion relations cross, regardless of the field value. When μB reaches the maximum allowed value, instability takes place at $q = 0$. That destabilizes the system to transform into a y-parallel state, which is the only available structure connected by a $q = 0$ perturbation.

Further results are shown in Fig. 5 for $K_1 = 2.02847D$, $K_3 = 0$, where a field *is needed* to stabilize the state. One sees a limited range of field that can accomplish that. At this value of K_1, the maximum possible field where the oblique state is maintained stable is $\mu B_{\max} \approx 3.1554D$. This pair of (K_1, B) values constitutes a type of triple point, where oblique, y-parallel, and y-alternating states are all nominally stable, see Fig. 13 later. At the maximum allowed field, the instability takes place at $q = 0$, showing the tendency to transform into a y-parallel state. To the contrary, at the minimum required field, the instability takes place at $qa = \pi$, indicating a transformation into a y-alt state.

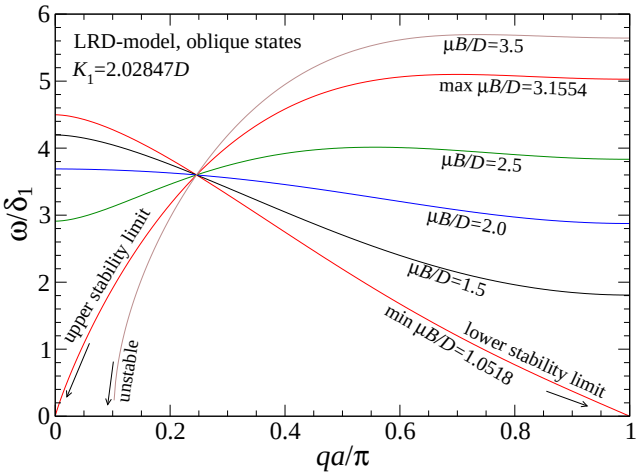

FIG. 5: Mode frequencies from Eq. (39) in the LRD-model for oblique states with $K_1 = 2.02847D$, $K_3 = 0$, with a transverse applied field strength as indicated. The field $\mu B/D$ must be between required minimum and maximum values for stability at this anisotropy strength. The state transforms to y-par if $\mu B > \mu B_{\rm max}$ and to y-alt if $\mu B < \mu B_{\rm min}$. This anisotropy value is that for the triple point of the system, see Fig. 13.

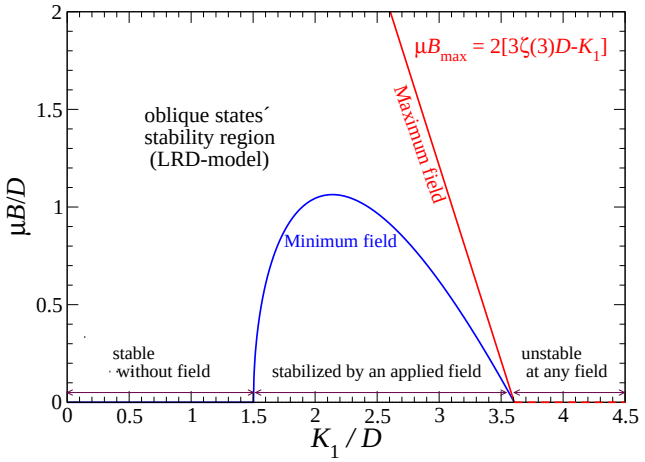

FIG. 6: For oblique states with LRD interactions, the minimum and maximum applied field strength μB required for stabilization, as a function of the in-plane anisotropy K_1, both relative to dipolar coupling D, as given in Eqs. (56) and (57) with $R \to \infty$.

3. *General stability of oblique states*

Stability of oblique states has two requirements. The first is that $\lambda_\phi(q) > 0$ for any value of wavevector q. Physically, the tendency of an oblique state to destabilize occurs at $qa \approx \pi$, because that type of perturbation deforms it towards an available y-alternating state. This can also be seen by realizing that $\lambda_\phi(q)$ becomes smallest at $qa = \pi$, because that makes the terms with odd k in the Clausen sums in Eq. 52 negative. Enforcing this first constraint, stability requires

$$\sin^2\phi^{(0)} > \frac{K_1 - [2\zeta_R + \mathrm{Cl}_{R,3}(\pi)]D}{K_1 - 3\mathrm{Cl}_{R,3}(\pi)D}. \qquad (55)$$

But the equilibrium angle is determined by the applied field, so using (11) this translates into a requirement on the applied field,

$$\mu B > 2(3\zeta_R D - K_1)\sqrt{\frac{K_1 - [2\zeta_R + \mathrm{Cl}_{R,3}(\pi)]D}{K_1 - 3\mathrm{Cl}_{R,3}(\pi)D}}. \qquad (56)$$

For the LRD model, this expression requires $K_1 > 2\zeta(3) + \mathrm{Cl}_3(\pi) = (5/4)\zeta D \approx 1.50257\ D$, which is the zero-field anisotropy limit, see the x-parallel data in Fig. 9 of Ref. [18].

The second requirement for stability is that $s_0 < 1$, otherwise, the system would transform into y-parallel. This would take place at $qa = 0$, or, applying the result (11) and solving for the allowed field,

$$\mu B < 2(3\zeta_R D - K_1). \qquad (57)$$

The right hand side is the upper limit for allowed applied field. It also implies that oblique states do not exist if $K_1 > 3\zeta_R D$, for any applied field. In the LRD model, the region with $1.50257D < K_1 < 3.60617D$ requires a field for stabilization. The limited range of allowed field and anisotropy for the LRD model is indicated in Fig. 6.

These results show two things: (1) An applied field extends the range of stability of oblique states to higher in-plane anisotropy values (K_1) compared to x-parallel states with no applied field, and (2) there is a limited range of applied field that will stabilize oblique states, which depends only on the in-plane anisotropy. Outside of this required range of μB, the system will either transform to a y-alternating state (μB too small) or to a y-parallel state (μB too large).

D. Linearized analysis of y-parallel states

Continue with y-parallel states, and consider their energy changes when small deviations of the dipoles take place, followed by an analysis of stability and dynamics.

1. *Expanding H for y-parallel states*

For a y-parallel state with replacement $\phi_n \to p\frac{\pi}{2} + \phi_n$, the Hamiltonian can be expanded to quadratic order in the deviations ϕ_n, θ_n, as follows. The dipolar pair energy of site n interacting with site $n+k$ is

$$H^D_{n,k} = \frac{D}{k^3}\Big(1 - \tfrac{1}{2}\phi_n^2 - \tfrac{1}{2}\phi_{n+k}^2 - 2\phi_n\phi_{n+k} - \tfrac{1}{2}\theta_n^2 - \tfrac{1}{2}\theta_{n+k}^2 + \theta_n\theta_{n+k}\Big). \qquad (58)$$

This is summed over all n and only $k \geq 1$ to get the total dipolar energy. In addition, there are anisotropy terms,

$$H^K_n = -K_1\left(1 - \phi_n^2 - \theta_n^2\right) + K_3\theta_n^2, \qquad (59)$$

and field terms,

$$H_n^B = -p\mu B\left(1 - \tfrac{1}{2}\phi_n^2 - \tfrac{1}{2}\theta_n^2\right). \quad (60)$$

The combination of these parts gives the per-site Hamiltonian with zeroth and quadratic order parts, $H_n = H_n^{(0)} + H_n^{(2)}$,

$$H_n^{(0)} = D\sum_{k=1}^{R}\frac{1}{k^3} - K_1 - p\mu B = \zeta_R D - K_1 - p\mu B, \quad (61)$$

which agrees with Eq. (15), and

$$H_n^{(2)} = D\sum_{k=1}^{R}\frac{1}{k^3}\left(-\phi_n^2 - 2\phi_n\phi_{n+k} - \theta_n^2 + \theta_n\theta_{n+k}\right) + K_1\phi_n^2 + (K_1+K_3)\theta_n^2 + \tfrac{1}{2}p\mu B(\phi_n^2+\theta_n^2). \quad (62)$$

In-plane and out-of-plane deviation energies are completely decoupled. The on-site matrix elements of $\boldsymbol{M}_\phi$ and $\boldsymbol{M}_\theta$ are the coefficients of ϕ_n^2 and θ_n^2 in $H_n^{(2)}$,

$$M_{\phi,n,n} = -\zeta_R D + K_1 + \tfrac{1}{2}p\mu B,$$
$$M_{\theta,n,n} = -\zeta_R D + K_{13} + \tfrac{1}{2}p\mu B, \quad (63)$$

where the net out-of-plane anisotropy strength is

$$K_{13} \equiv K_1 + K_3. \quad (64)$$

The inter-site matrix elements are half the coefficients of $\phi_n\phi_{n+k}$ and $\theta_n\theta_{n+k}$ in $H_n^{(2)}$,

$$M_{\phi,n,n+k} = -\frac{D}{k^3}, \quad M_{\theta,n,n+k} = \frac{D}{2k^3}. \quad (65)$$

The system is symmetric along the chain, so there are the same matrix elements for $n, n-k$ bonds.

2. *Energy and frequency eigenvalues of y-parallel states*

The energy eigenvalues for small deviations control dynamics and determine stability. For an in-plane deviation, the matrix elements substituted into Eq. (42) give the eigenvalues,

$$\lambda_\phi(q) = -\zeta_R D - 2D\sum_{k=1}^{R}\frac{\cos kqa}{k^3} + K_1 + \tfrac{1}{2}p\mu B. \quad (66)$$

A similar expression is found for the eigenvalues associated with out-of-plane deviations,

$$\lambda_\theta(q) = -\zeta_R D + D\sum_{k=1}^{R}\frac{\cos kqa}{k^3} + K_{13} + \tfrac{1}{2}p\mu B. \quad (67)$$

Both increase linearly with the field factor, $p\mu B$.

A first example of the mode frequencies resulting from Eq. (39) is shown in Fig. 7 for $K_1 = 1D$ with a y-parallel state with polarization $p = +1$. A large positive field (aligned with the polarization direction of the state) will not destabilize it. To the contrary, there is a minimum positive applied field (same as the polarization direction, of value $\mu B/D \approx 5.21234$) below which the state is destabilized by $q = 0$ fluctuations, presumably into an oblique state, that being the only available stable state for this low value of K_1.

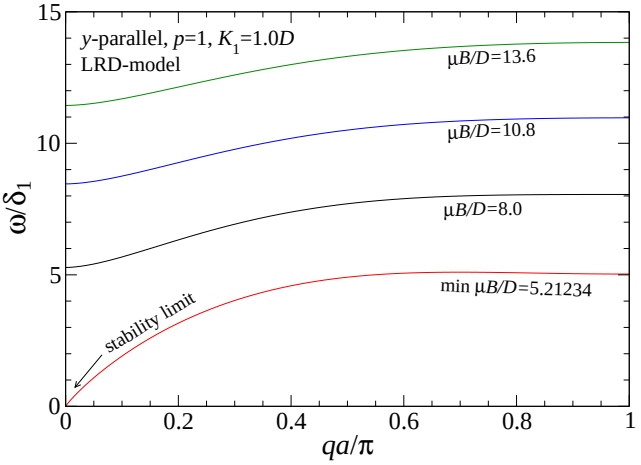

FIG. 7: Mode frequencies from Eq. (39) in the LRD-model ($R \to \infty$) for y-parallel states with $K_1 = 1.0D$, $K_3 = 0, p = +1$, with transverse applied field strength as indicated. The field $\mu B/D$ must be above a required minimum for $p = +1$ y-parallel stability, but any large positive field is allowed. If $\mu B/D$ is below the stability limit, the chain will transform into an oblique state because the $q = 0$ fluctuations will only connect to that state structure at this value of K_1.

A second example of the mode frequencies is shown in Fig. 8 for $K_1 = 5D$ and a y-parallel state with polarization $p = +1$. A large positive field (aligned with the polarization direction of the state) will not destabilize it. To the contrary, there is a minimum applied field (opposite to the polarization direction, or negative, of value $\mu B/D \approx -2.787$) below which the state is destabilized by $q = 0$ fluctuations into the other y-parallel state with $p = -1$. (The only other available state would be y-alt, but that does not connect to y-parallel via a $q = 0$ fluctuation.) Note the vivid similarity to Fig. 7: the curves are nearly the same shapes, because equal field increments are used in the curves, starting from the minimum required for stability at the applied value of K_1, see Eqs. (66) and (67), where the frequencies shift equivalently with a change in K_1 as with a change in $\frac{1}{2}p\mu B$.

3. *General stability of y-parallel states*

The y-parallel states are stable if the energy eigenvalues λ_ϕ and λ_θ remain positive, for any wave-like deviation (i.e., for all possible wavevectors q). At the minimum applied field for which y-parallel exists, the frequency goes to zero at $q \approx 0$, see Figs. 7 and 8. This implies that a

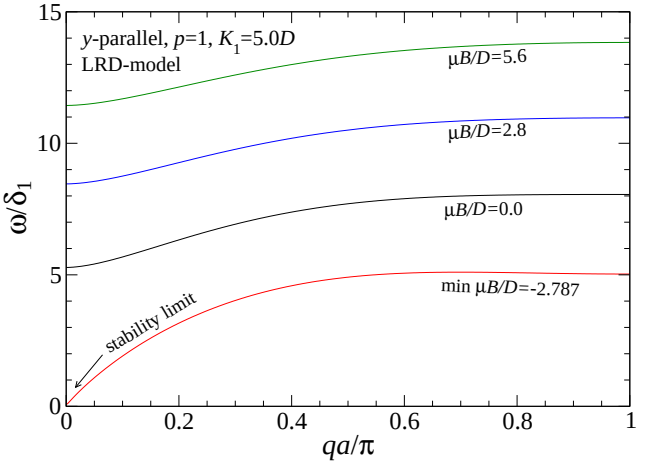

FIG. 8: Mode frequencies from Eq. (39) in the LRD-model for y-parallel states with $K_1 = 5D$, $K_3 = 0, p = +1$, with transverse applied field strength as indicated. The field $\mu B/D$ must be above a required minimum for $p = +1$ y-parallel stability, but any large positive field is allowed. If $\mu B/D$ is below the stability limit, the state will transform into $p = -1$ y-parallel because the $q = 0$ fluctuations will only connect to that state structure.

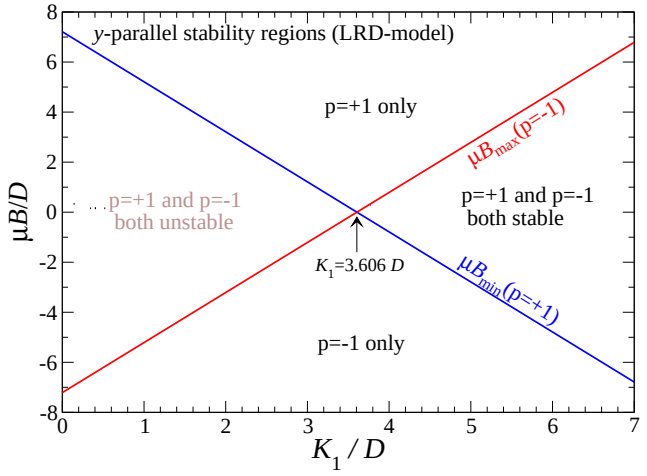

FIG. 9: For a y-parallel state with LRD interactions ($R \to \infty$), the field μB required for stabilization, as a function of the in-plane anisotropy K_1, taking $K_3 = 0$. The minimum field required for $p = +1$ appears in Eq. (70); the maximum field for $p = -1$ appears in Eq. (71), where p indicates the polarization direction ($\pm\hat{y}$).

y-parallel state might have a long-wavelength deviation that would tend to rotate it into another allowed state Noting that $\mathrm{Cl}_{R,3}(0) = \zeta_R$, the eigenvalues at $q = 0$ are

$$\lambda_\phi(0) = K_1 + \tfrac{1}{2}p\mu B - 3\zeta_R D,$$
$$\lambda_\theta(0) = K_{13} + \tfrac{1}{2}p\mu B. \tag{68}$$

Assuming these must be positive for stability, they give requirements on the applied field,

$$\lambda_\phi(0) > 0 \implies p\mu B > 2(3\zeta_R D - K_1),$$
$$\lambda_\theta(0) > 0 \implies p\mu B > -2K_{13}. \tag{69}$$

The requirement from $\lambda_\phi(0) > 0$ is more restrictive and is the deciding factor. Therefore, when the dipoles are aligned with $\mathbf{B}$, the allowed field range is

$$\mu B > 2(3\zeta_R D - K_1), \quad p = +1. \tag{70}$$

If the y-parallel state has dipoles pointing opposite to $\mathbf{B}$, which is much higher energy, the field constraint is

$$\mu B < -2(3\zeta_R - K_1), \quad p = -1. \tag{71}$$

One can also consider deviations at $qa = \pi$, which might connect the state to y-alternating structure, but that gives constraints already satisfied by the requirements from $\lambda_\phi(0) > 0$. There is no tendency for y-parallel to destabilize into an alternating structure.

The resulting stable regions for y-parallel states with infinite-range dipole interactions are depicted in Fig. 9. Around a central point at $K_1 \approx 3.606D$, $B = 0$, there are four distinct regions: a forbidden region with $K_1 < 3.606D$ where neither is stable, two exclusive regions where only one of the polarizations is stable, and a bistable region with $K_1 > 3.606D$ where both polarization are stable.

E. Linearized analysis of y-alternating states

For y-alternating states, the analysis requires a two-sublattice model: sites at even (odd) n are considered to be on the A (B) sublattice. When a field is applied, symmetry is broken, making the two sublattices inequivalent, and the theory requires different deviation waves on the two sublattices. Further, the dynamic frequency eigenvalues now are not given by Eq. (39), but another expression, due to the symmetry breaking by the field.

1. *Expanding H for y-alternating states*

For y-alt states, the equilibrium in-plane angles on the two sublattices are $\phi_A^{(0)} = p\frac{\pi}{2}$ and $\phi_B^{(0)} = -p\frac{\pi}{2}$, where polarization $p = \pm 1$ to give two y-alt states. With deviations, the in-plane angles are replaced by

$$\phi_n \to (-1)^n p\frac{\pi}{2} + \phi_n, \tag{72}$$

where ϕ_n are now the small deviations from the equilibrium y-alt state. With θ_n being the out-of-plane deviation at a site, the contributions to H can be expanded to quadratic order in the angles.

Consider dipolar interactions. Site n is on one sublattice. Then site $n + k$ with k odd belongs to the other sublattice ($n, n+k$ is an AB bond). Their pair contribution to H, up to quadratic order, is found to be

$$H^D_{n,k} \approx \frac{D}{k^3}\big(-1 + \tfrac{1}{2}\phi_n^2 + \tfrac{1}{2}\phi_{n+k}^2 + 2\phi_n\phi_{n+k}$$
$$+ \tfrac{1}{2}\theta_n^2 + \tfrac{1}{2}\theta_{n+k}^2 + \theta_n\theta_{n+k}\big), \quad k = \text{odd}. \tag{73}$$

On the other hand, when k is even, the pair is on the same sublattice (AA or BB bonds), and the contribution is different,

$$H^D_{n,k} \approx \frac{D}{k^3}\big(1 - \tfrac{1}{2}\phi_n^2 - \tfrac{1}{2}\phi_{n+k}^2 - 2\phi_n\phi_{n+k} - \tfrac{1}{2}\theta_n^2 - \tfrac{1}{2}\theta_{n+k}^2 + \theta_n\theta_{n+k}\big), \quad k = \text{even}. \tag{74}$$

In the full Hamiltonian, each $(n, n+k)$ pair should be counted once. These are equivalent to a *single* expression for any n, k, with $k \geq 1$, whose sum contributes to H,

$$H^D_{n,k} \approx \frac{D}{k^3}\big[(-1)^k\big(1 - \phi_n^2 - 2\phi_n\phi_{n+k} - \theta_n^2\big) + \theta_n\theta_{n+k}\big], \quad k \geq 1. \tag{75}$$

There are also anisotropy terms,

$$H^K_n \approx -K_1(1 - \phi_n^2 - \theta_n^2) + K_3\theta_n^2. \tag{76}$$

The field terms for both sublattices can be expressed succinctly,

$$H^B_n \approx -(-1)^n p\mu B(1 - \tfrac{1}{2}\phi_n^2 - \tfrac{1}{2}\theta_n^2). \tag{77}$$

The combination of dipolar, anisotropy and field terms produces the per-site Hamiltonian, which is composed from zeroth and second order parts: $H_n \approx H^{(0)}_n + H^{(2)}_n$. The zeroth order term reproduces the per-site equilibrium energy $u_{y\text{-alt}}$ in (23), independent of the field,

$$H^{(0)}_n = D\sum_{k=1}^{R}\frac{(-1)^k}{k^3} - K_1 = D\mathrm{Cl}_{R,3}(\pi) - K_1. \tag{78}$$

There remains the quadratic parts,

$$H^{(2)}_n = D\sum_{k=1}^{R}\frac{1}{k^3}\big[(-1)^k\big(-\phi_n^2 - 2\phi_n\phi_{n+k} - \theta_n^2\big) + \theta_n\theta_{n+k}\big] + K_1(\phi_n^2 + \theta_n^2) + K_3\theta_n^2 + (-1)^n\tfrac{1}{2}p\mu B(\phi_n^2 + \theta_n^2). \tag{79}$$

Using the matrix notation of Eq. (32), the on-site matrix elements alternate by site due to the field,

$$M_{\phi,n,n} = -D\mathrm{Cl}_{R,3}(\pi) + K_1 + (-1)^n\tfrac{1}{2}p\mu B,$$
$$M_{\theta,n,n} = -D\mathrm{Cl}_{R,3}(\pi) + K_{13} + (-1)^n\tfrac{1}{2}p\mu B. \tag{80}$$

The inter-site elements come from the pair terms in $H^{(2)}_n$,

$$M_{\phi,n,n+k} = -D\frac{(-1)^k}{k^3}, \quad M_{\theta,n,n+k} = \frac{D}{2k^3}. \tag{81}$$

These resemble the y-parallel matrix elements, except for the alternation with separation k in $M_{\phi,n,n+k}$.

2. *Frequency eigenvalues of y-alternating states*

Although the energy eigenvalues of $\boldsymbol{M}_\phi$ and $\boldsymbol{M}_\theta$ can be found, they do not play a direct role in the expressions for the frequency eigenvalues of y-alternating states. Instead, we inspect the dynamics that results from (33), assuming inversion symmetry and separating out the on-site interaction,

$$-\mathrm{i}\omega\frac{\mu}{\gamma_\mathrm{e}}\phi_n = 2\big\{M_{\theta,n,n}\theta_n + \sum_{k=1}^{R}M_{\theta,n,n+k}(\theta_{n-k} + \theta_{n+k})\big\},$$
$$-\mathrm{i}\omega\frac{\mu}{\gamma_\mathrm{e}}\theta_n = -2\big\{M_{\phi,n,n}\phi_n + \sum_{k=1}^{R}M_{\phi,n,n+k}(\phi_{n-k} + \phi_{n+k})\big\}. \tag{82}$$

A two-sublattice traveling wave expression is assumed,

$$(\phi_n, \theta_n) = \begin{cases}(a_\phi, a_\theta)e^{\mathrm{i}(qna-\omega t)} & n = \text{even, A-sites,}\\ (b_\phi, b_\theta)e^{\mathrm{i}(qna-\omega t)} & n = \text{odd, B-sites.}\end{cases} \tag{83}$$

Substituted into (33), there results a pair of coupled 2×2 matrix equations, similar to those appearing in analysis of remanent states of square-lattice ASI [12],

$$-\mathrm{i}\omega\begin{pmatrix}a_\phi\\ b_\phi\end{pmatrix} = \begin{pmatrix}m_{aa} & m_{ab}\\ m_{ba} & m_{bb}\end{pmatrix}\begin{pmatrix}a_\theta\\ b_\theta\end{pmatrix},$$
$$-\mathrm{i}\omega\begin{pmatrix}a_\theta\\ b_\theta\end{pmatrix} = -\begin{pmatrix}n_{aa} & n_{ab}\\ n_{ba} & n_{bb}\end{pmatrix}\begin{pmatrix}a_\phi\\ b_\phi\end{pmatrix}. \tag{84}$$

The elements of the 2×2 matrices $\boldsymbol{m}$ and $\boldsymbol{n}$ come from projecting $\boldsymbol{M}_\theta$ and $\boldsymbol{M}_\phi$ onto the two-sublattice traveling wave, such as the matrix $\boldsymbol{m}$ due to θ variations,

$$m_{aa} = 2\frac{\gamma_\mathrm{e}}{\mu}\big[M_{\theta,AA} + \sum_{k=\text{even}}^{R}2M_{\theta,n,n+k}\cos kqa\big],$$
$$m_{bb} = 2\frac{\gamma_\mathrm{e}}{\mu}\big[M_{\theta,BB} + \sum_{k=\text{even}}^{R}2M_{\theta,n,n+k}\cos kqa\big],$$
$$m_{ab} = m_{ba} = 2\frac{\gamma_\mathrm{e}}{\mu}\sum_{k=\text{odd}}^{R}2M_{\theta,n,n+k}\cos kqa. \tag{85}$$

The symbols $M_{\theta,AA}$ and $M_{\theta,BB}$ indicate the on-site matrix elements for each sublattice (they differ in the field term). The sums, due to dipole pair interactions, are over positive values of k and are independent of the choice of a central site n. The cosines result from adding interactions in both directions,

$$e^{\mathrm{i}qka} + e^{\mathrm{i}q(-k)a} = 2\cos kqa. \tag{86}$$

Using the known matrix elements of $\boldsymbol{M}_\theta$ from (80) and (81), these are

$$m_{aa} = 2\big\{D[\mathrm{Cl}_{3\mathrm{e}}(qa) - \mathrm{Cl}_3(\pi)] + K_{13} + \tfrac{1}{2}p\mu B\big\},$$
$$m_{bb} = 2\big\{D[\mathrm{Cl}_{3\mathrm{e}}(qa) - \mathrm{Cl}_3(\pi)] + K_{13} - \tfrac{1}{2}p\mu B\big\},$$
$$m_{ab} = m_{ba} = 2D\,\mathrm{Cl}_{3\mathrm{o}}(qa), \tag{87}$$

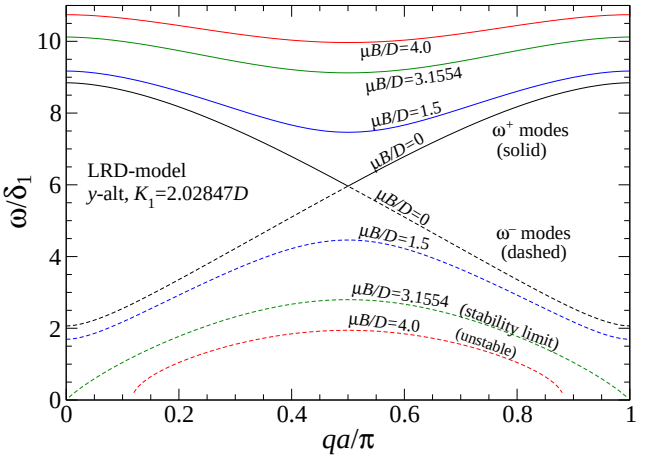

FIG. 10: For a y-alternating state in the LRD-model, typical dispersion relations for $K_1/D = 2.02847$, $K_3 = 0$, at indicated field strengths μB, as obtained from Eq. 92. Note the instability when μB surpasses its upper allowed value of $3.1554D$ (the triple point for the three phases, see Fig. 13), beyond which the state should transform into y-parallel.

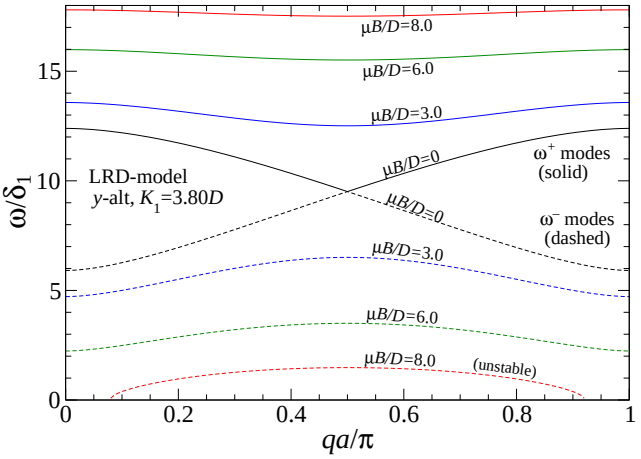

FIG. 11: For a y-alternating state in the LRD-model, typical dispersion relations for $K_1/D = 3.80$, $K_3 = 0$, at indicated field strengths μB, as obtained from Eq. 92. Instability occurs for $\mu B > 7.73147D$, see Eq. (99) and Fig. 13, beyond which the state should transform into y-parallel.

which depend on even-term and odd-term Clausen sums,

$$\mathrm{Cl}_{3\mathrm{e}}(qa) = \sum_{k=\mathrm{even}}^{R} \frac{\cos kqa}{k^3}, \quad \mathrm{Cl}_{3\mathrm{o}}(qa) = \sum_{k=\mathrm{odd}}^{R} \frac{\cos kqa}{k^3}. \tag{88}$$

The matrix $\boldsymbol{n}$ due to ϕ variations has similar structure,

$$\begin{aligned} n_{aa} &= 2\frac{\gamma_\mathrm{e}}{\mu}\big[M_{\phi,AA} + \sum_{k=\mathrm{even}}^{R} 2M_{\phi,n,n+k}\cos kqa\big], \\ n_{bb} &= 2\frac{\gamma_\mathrm{e}}{\mu}\big[M_{\phi,BB} + \sum_{k=\mathrm{even}}^{R} 2M_{\phi,n,n+k}\cos kqa\big], \\ n_{ab} &= n_{ba} = 2\frac{\gamma_\mathrm{e}}{\mu}\sum_{k=\mathrm{odd}}^{R} 2M_{\phi,n,n+k}\cos kqa. \end{aligned} \tag{89}$$

Using the matrix elements from (80) and (81), these become

$$\begin{aligned} n_{aa} &= 2\big\{D[-2\mathrm{Cl}_{3\mathrm{e}}(qa) - \mathrm{Cl}_3(\pi)] + K_1 + \tfrac{1}{2}p\mu B\big\}, \\ n_{bb} &= 2\big\{D[-2\mathrm{Cl}_{3\mathrm{e}}(qa) - \mathrm{Cl}_3(\pi)] + K_1 - \tfrac{1}{2}p\mu B\big\}, \\ n_{ab} &= n_{ba} = 4D\,\mathrm{Cl}_{3\mathrm{o}}(qa). \end{aligned} \tag{90}$$

The frequency eigenvalues can be obtained either by eliminating say, the (a_θ, b_θ) amplitudes from (84), and solving a 2×2 reduced system, or, keeping all four amplitudes and solving the 4×4 eigenvalue problem equivalent to (84), expressed as

$$\begin{pmatrix} 0 & 0 & & \\ 0 & 0 & \multicolumn{2}{c}{\boldsymbol{m}} \\ & & 0 & 0 \\ \multicolumn{2}{c}{\boldsymbol{n}} & 0 & 0 \end{pmatrix} \begin{pmatrix} a_\phi \\ b_\phi \\ \mathrm{i}a_\theta \\ \mathrm{i}b_\theta \end{pmatrix} = \omega \begin{pmatrix} a_\phi \\ b_\phi \\ \mathrm{i}a_\theta \\ \mathrm{i}b_\theta \end{pmatrix}. \tag{91}$$

It is a straightforward exercise [12] to obtain the eigenvalues of the 4×4 matrix on the LHS, which are given from

$$(\omega^\pm)^2 = \tfrac{1}{2}\left[(\boldsymbol{m}^\dagger\cdot\boldsymbol{n}) \pm \sqrt{(\boldsymbol{m}^\dagger\cdot\boldsymbol{n})^2 - 4|\boldsymbol{m}||\boldsymbol{n}|}\right]. \tag{92}$$

The dots indicate term-by-term scalar products of the 2×2 matrices ($\boldsymbol{m}^\dagger\cdot\boldsymbol{n} = \sum_{i,j} m_{ij}n_{ji}$), and $|\boldsymbol{m}||\boldsymbol{n}|$ is the product of their determinants. We calculate the two frequencies with positive real parts, which give waves traveling in the positive x-direction. When the applied field B is zero, it is possible to show that the frequency eigenvalues are given by an expression equivalent to Eq. (39), namely,

$$(\omega^\pm)^2 = \lambda^\pm_{\boldsymbol{m}}\lambda^\pm_{\boldsymbol{n}}, \tag{93}$$

where the eigenvalues of the $\boldsymbol{m}$ and $\boldsymbol{n}$ matrices enter on the RHS. Once the field is nonzero, however, this form does not hold. A simple expression in terms of the energy eigenvalues has not been found.

Some typical dispersion relations are shown in Fig. 10, for the triple point anisotropy value, $K_1/D = 2.02847$, which has instability for $\mu B/D > 3.1554$. The instability is driven both at $qa = 0$ and at $qa = \pi$, and should transform the state into y-parallel once μB is above this limit. A similar behavior appears for $K_1/D = 3.80$ as shown in Fig. 11, which allows for much stronger field before instability takes place. Note that the frequencies do not depend on the phase-like parameter p, which only determines whether even or odd sites are aligned with the field.

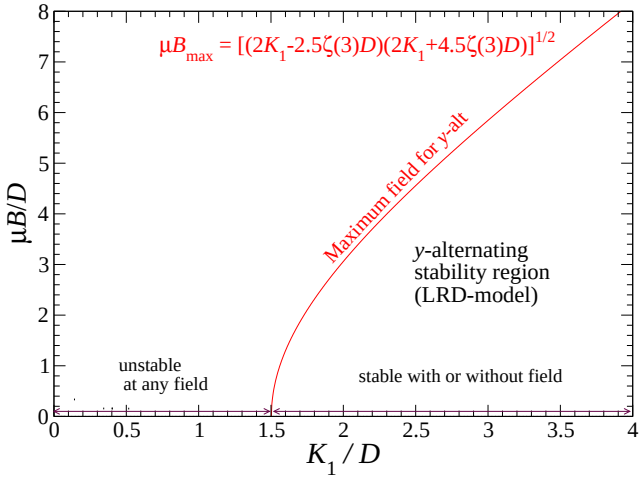

FIG. 12: For a y-alternating state with LRD interactions, the maximum applied field strength μB below which the state is stable, and overall stability region, as a function of relative in-plane anisotropy K_1/D, as given in Eq. (99). This is based on requiring positive energy eigenvalues, especially $\lambda_{\boldsymbol{n}}^{-} > 0$.

3. *General stability of y-alternating states*

If any frequency eigenvalue from Eq. (92) for any value of q becomes negative or imaginary, the y-alternating state is unstable. However, it is mathematically difficult to apply this principle for determining the range of applied field for which the state will remain stable.

Instead, we again use the principle that real and positive energy eigenvalues are required for stability. Instability due to deviations in ϕ or θ is indicated by negative energy eigenvalues, signifying that the state can lower its energy and destabilize to a different state. The point where an eigenvalue is zero gives a limiting value for the applied field, for the given anisotropy values. This principle can be applied to the $\boldsymbol{m}$ and $\boldsymbol{n}$ matrices, even though it has not been possible to write the frequencies in terms of energy eigenvalues for y-alt states.

The matrices $\boldsymbol{m}$ and $\boldsymbol{n}$ have this form which highlights the field dependence:

$$\boldsymbol{n} = \begin{pmatrix} n_{aa} & n_{ab} \\ n_{ba} & n_{bb} \end{pmatrix} = \begin{pmatrix} n_{aa}^0 + p\mu B & n_{ab} \\ n_{ba} & n_{aa}^0 - p\mu B \end{pmatrix}, \quad (94)$$

where $= n_{aa}^0$ is the zero-field diagonal matrix element, and $n_{ab} = n_{ba}$ is independent of the field. A brief calculation gives the two eigenvalues,

$$\lambda_{\boldsymbol{n}}^{\pm} = n_{aa}^0 \pm \sqrt{n_{ab}^2 + (\mu B)^2}, \quad (95)$$

with a similar expression for the pair of $\lambda_{\boldsymbol{m}}^{\pm}$ eigenvalues. Then the stability requirement $\lambda_{\boldsymbol{n}}^{\pm} > 0$ gives a constraint on the applied field magnitude,

$$\mu B < \sqrt{(n_{aa}^0)^2 - n_{ab}^2}. \quad (96)$$

Inspecting the typical dispersion relations in the examples in Figs. 10 and 11, the instability is initiated equally at $q = 0$ and at $qa = \pi$. At $q = 0$, the sums needed in the matrix elements for infinite range interactions are

$$\mathrm{Cl}_{3\mathrm{e}}(0) = \sum_{k=\mathrm{even}} \frac{1}{k^3} = \sum_{n=1}^{\infty} \frac{1}{(2n)^3} = \tfrac{1}{8}\zeta(3),$$
$$\mathrm{Cl}_{3\mathrm{o}}(0) = \sum_{k=\mathrm{odd}} \frac{1}{k^3} = \mathrm{Cl}_3(0) - \mathrm{Cl}_{3\mathrm{e}}(0) = \tfrac{7}{8}\zeta(3). \quad (97)$$

Then the matrix elements for $q = 0$ are found to be

$$n_{aa}^0 = \zeta(3)D + 2K_1, \qquad n_{ab} = \tfrac{7}{2}\zeta(3)D. \quad (98)$$

Then this implies a requirement on the applied field, for the LRD model,

$$\mu B < \sqrt{\left(2K_1 - \tfrac{5}{2}\zeta(3)D\right)\left(2K_1 + \tfrac{9}{2}\zeta(3)D\right)}. \quad (99)$$

The same result is obtained from $\boldsymbol{n}(\pi)$. The calculation can also be repeated for the eigenvalues $\lambda_{\boldsymbol{m}}^{\pm}$, which leads to a second constraint on the field,

$$\mu B < \sqrt{2K_{13}\left(2K_{13} + \tfrac{7}{2}\zeta(3)D\right)}. \quad (100)$$

However, the limiting field due to $\lambda_{\boldsymbol{n}}^{\pm}$ is smaller and more restrictive than this, and it determines stability. Therefore, the maximum field for stable y-alt solutions is given by Eq. (99). That result is plotted in Fig. 12. Also, y-alt states require a minimum in-plane anisotropy; stability is only possible in the LRD model if

$$K_1 > \tfrac{5}{4}\zeta(3)D. \quad (101)$$

If the applied field falls somewhere in the region above or to the left of the maximum allowed curve in Fig. 12, then the possible stable states it can transform into are either oblique (for lower anisotropy K_1) or y-parallel (for larger values of K_1). This statement is made more precise in the next section.

V. SUMMARY ON STABILITY AND TRANSFORMATIONS

Stability has been determined for the three states studied (oblique, y-par and y-alt) based on requirements of positive energy eigenvalues, for in-plane and out-of-plane dipole fluctuations. The stable ranges of applied field combined with anisotropy K_1 have been determined in the LRD model ($R \to \infty$), for the particular case of vanishing easy-plane anisotropy, $K_3 = 0$. The stable regions are indicated in a single phase-like diagram in Fig. 13 in the field-anisotropy (μB-K_1) plane. Each state has an exclusionary region where it is the only stable state: oblique state only for low B and low K_1, y-par only for high B and low K_1, and y-alt only for low B and intermediate K_1. The states also have metastable regions shared

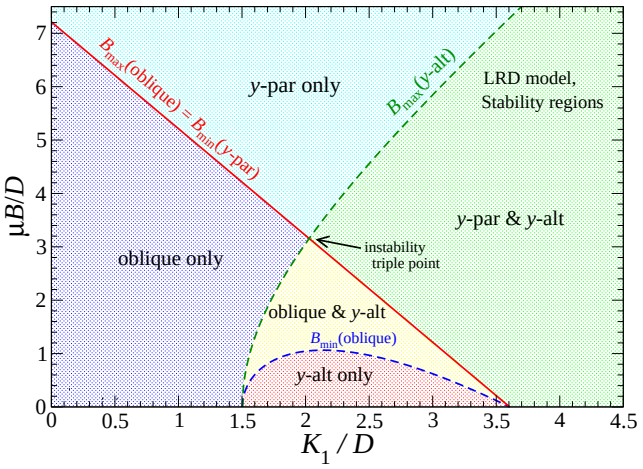

FIG. 13: Diagram of the field/anisotropy regions of the LRD-model where the different states are stable, as determined from having positive energy eigenvalues, especially $\lambda_{\boldsymbol{n}}^{-}$. Solid curves indicate an imperative change of state across the curve (oblique/y-par); dashed curves indicate that only one state is unstable when crossing that curve.

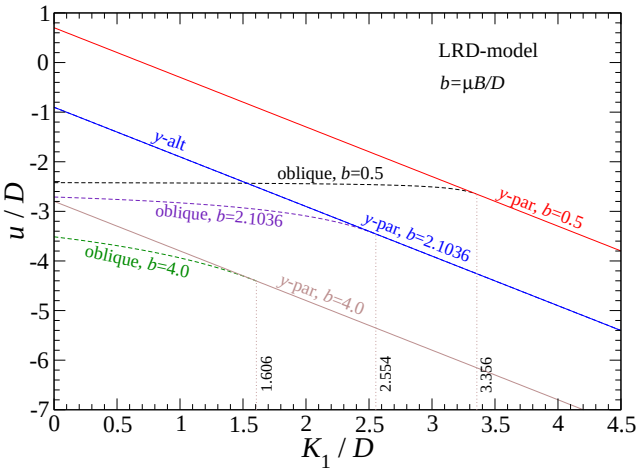

FIG. 14: Per-site energies of the states with LRD, from Eqs. (12), (15), and (26), for indicated dimensionless field values $b = \mu B/D$, versus in-plane anisotropy, with $K_3 = 0$. Note that oblique becomes the same as y-parallel where the two curves meet. The y-alt energy does not depend on b. The y-alt line matches the y-par energy line for $b = 2.1036$, where those two states are equal in energy for all K_1.

with another of the states. There are only dual-state regions and no triple-state region. Notably, oblique and y-par are mutually exclusive, except along their boundary (the solid red line).

Crossing any of the curves in Fig. 13 indicates a possible transformation of the system, due to instability, from one of the states to another. Dashed curves are used to indicate that only one of the states becomes unstable crossing the curve, while the other one is stable on both sides. If the state is allowed on both sides of a curve, then it does not transform when crossing the curve.

Crossing over the solid red line in Fig. 13, oblique must transform into y-par or *vice-versa* in the other direction. This conclusion is reached because these processes destabilize the original state with fluctuations at $q = 0$, see the dispersion relations in Figs. 4 and 7. Oblique will not transform to y-alt by crossing over the solid red line, because it does not have a destabilizing fluctuation there at $qa = \pi$. Instead, transformation from oblique to y-alt *can* take place by crossing downward over the blue dashed curve (minimum field for oblique state stability), which occurs with a $qa = \pi$ fluctuation, as seen in Fig. 5. One could also begin in a y-alt state and cross over the green dashed curve, transforming either into oblique or y-par.

There is a central point where the red line crosses the green curve in Fig. 13 where all the phases become unstable as the point is crossed, which might be termed an *instability triple point*. Starting in oblique and moving through that point gives y-par. Starting in y-par and moving through the point gives back oblique. Starting in y-alt and moving through the point vertically gives y-par, and moving through horizontally gives oblique. The point is located by setting the expressions for the two curves equal, which gives

$$\frac{K_1}{D} = \tfrac{189}{112}\zeta(3) \approx 2.02847, \quad \frac{\mu B}{D} = \tfrac{147}{56}\zeta(3) \approx 3.1554. \tag{102}$$

It should be a point of strong fluctuations, as the system cannot easily decide which state to choose.

VI. COMPARING THE STATES' ENERGIES PER SITE

Due to metastability in this system, comparison of energy per site between states is not a good indicator of stability. An idea of this is given in Fig. 14 for the LRD model, which shows the states' energies per site u vs. anisotropy K_1, for different field values, similar to Fig. 9 for $B = 0$ in Ref. [18]. These are horizontal scans in the $(K_1, \mu B)$ phase diagram, Fig. 13, distinguished by dimensionless field $b \equiv \mu B/D$. The y-alt energy does not depend on the field, hence it has only one (straight-line) curve. The oblique state energy curves meet with the corresponding y-par curves at the maximum K_1 where there is a mandatory transformation into y-par. There is nothing in the curves to indicate where y-alt is stable or unstable, even though we know it has a limited stability range. The y-alt line matches the y-par line for $\mu B = (7/4)\zeta D \approx 2.1036D$.

In a better comparison, the regions where each of the three states has the lowest energy are determined, including LRD interactions, in contrast to the phase-like stability diagram in Fig. 13 based on positive energy eigenvalues. For example, the region where $u_{\text{oblq}} \leq u_{y\text{-par}}$ for

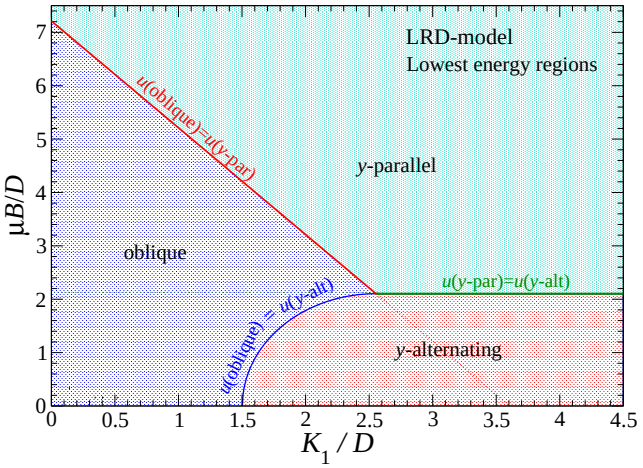

FIG. 15: Diagram of the field/anisotropy regions of the LRD model where the different states have the lowest energy per site u, from Eqs. (12), (15), and (26). Solid curves indicate where the primary states have equal energies; dashed curves indicate where secondary states have equal energies in that region. Oblique does not exist to the right of the solid and dotted red lines.

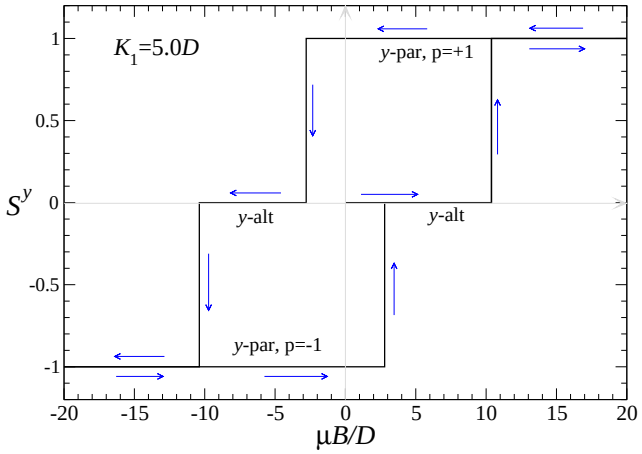

FIG. 16: The dimensionless magnetization per site S^y along the field direction, versus dimensionless applied field, for $K_1 = 5D$, $K_3 = 0$, starting from a y-alt state at $B = 0$, and then cycling B through positive and negative values. This is obtained from the LRD model's stability diagram, Fig. 13, using the y-alt stability limit, Eq. (99), and the y-par stability limits, Eqs. (70) and (71).

polarization $p = 1$ is found to be bounded by

$$\mu B = 2(3\zeta D - K_1), \tag{103}$$

which is the (red line) boundary in Fig. 13 based on energy eigenvalues. However, the region where $u_{\rm oblq} \leq u_{y\text{-alt}}$ is found to be

$$\mu B \geq 2\sqrt{(K_1 - \tfrac{5}{4}\zeta D)(3\zeta D - K_1)}, \tag{104}$$

and this is different from the (dashed blue) minimum field needed to stabilize oblique states. Finally, for y-par with $p = 1$, the region where $u_{y\text{-par}} \leq u_{y\text{-alt}}$ is given simply by

$$\mu B \geq \tfrac{7}{4}\zeta D \approx 2.1036D. \tag{105}$$

These results are combined into a diagram in Fig. 15 which shows the various regions where each state, including LRD interactions, has the lowest energy per site. In each of the three regions, there are at least two of the states possible. The only restriction, in principle, is that oblique and y-par are mutually exclusive. This diagram is notably different from the stability diagram in Fig. 13. Having the lowest energy alone does not determine stability. Stability is determined, indeed, by having finite frequency dynamic fluctuations over the whole range of allowed wavevectors.

VII. EFFECTS ON MAGNETIZATION

The stability diagram in Fig. 13 can be used to estimate how the dimensionless magnetization (S^y) behaves with applied field, and how that response depends on the anisotropy K_1. Measurement of the magnetization curves versus B could indicate the transitions among the states. The entire chain is assumed to be in one of the uniform states (after any transients). $K_3 = 0$ is assumed although any positive value will produce similar results.

For $K_1 < 1.50257D$ and $B = 0$, initially $S^y = 0$. As B increases positively, S^y will increase linearly as in Eq. (11), and the system will transform only between an oblique state and a y-par state. The transition occurs when the dipoles in the oblique state have rotated to be exactly parallel with $\mathbf{B}$, and $S^y \to 1$. There will be no hysteresis when B is reduced back through zero; the transitions are reversible.

For $1.50257 < K_1 < 3.606$, the system will naturally be in y-alt at $B = 0$, which is the lowest energy, with $S^y = 0$. As B is increased, eventually y-alt becomes unstable (at the green dashed curve in Fig. 13, Eq. 99) and there will be a transition either into an oblique state or y-par. That depends on where K_1 falls relative to the instability triple point. There will be a discontinuous change in S^y. The system will exhibit hysteresis when the field is later dropped back to zero and negative values.

For $K_1 > 3.606D$, which applies to more elongated islands, an example magnetization curve is shown in Fig. 16, for $K_1 = 5.0D$, $K_3 = 0$. The system might start in the lowest energy state, y-alt, at $B = 0$, with $S^y = 0$. It would stay in that state until B reaches the upper limit for y-alt stability [Eq. (99)], whereupon it transforms into y-par, with $S^y = 1$. Upon subsequent reduction of B to zero and negative values, there will be other discrete jumps and hysteresis. Note how the chain essentially becomes a three-level system in this case.

VIII. CONCLUSIONS

This model for a chain of interacting dipoles exposed to a transverse applied field possesses three uniform states (oblique, y-par and y-alt) that have metastable properties, depending of the interaction parameters and the field. The energy and frequency eigenvalues have been used to determine their stability regions in the parameter space. It is to be noted that stability is *not* associated with a state being of the lowest energy. The dynamic modes found give a direct indication of the type of destabilizing transformations that would take place when a stability limit is reached or surpassed.

In this problem, dipolar interactions help to stabilize the y-alternating states, even where they coexist with oblique and y-par states. In other systems, dipolar interactions generally influence the magnetic relaxation of chains of magnetic nanoparticles with randomly oriented anisotropy axes [30], and induce ordering in two-dimensional lattices of nanoparticles [31]. The results here will help to design new dipolar systems with desired switching transitions between metastable states. Variations on this problem may be especially useful for analysis of states in related systems, such as 2D artificial spin ices and other interacting dipole structures.

[1] Skjærvø S H, Marrows C H, Stamps R L and Heyderman L J, Advances in artificial spin ice, Nat. Rev. Phys. **2** 13 (2020).

[2] Nisoli C, Moessner R and Schiffer P, Colloquium: Artificial spin ice: Designing and imaging magnetic frustration, Rev. Mod. Phys. **85** 1473 (2013).

[3] Östman E, Arnalds U B, Kapaklis V, Taroni A and Hjøvarsson B, Ising-like behaviour of mesoscopic magnetic chains, J. Phys.: Condens. Matt. **30** 365301 (2018).

[4] Cisternas J *et al.*, Stable and unstable trajectories in a dipolar chain, Phys. Rev. B **103** 134443 (2021).

[5] Ising E, Beitrag zur Theorie des Ferromagnetismus, Z. Phys. **31** 253 (1925).

[6] Wysin G M, *Magnetic Excitations & Geometric Confinement: Theory and Simulations*, (London: IOP Expanding Physics ebook 2015).

[7] Wang R F, Nisoli C, Freitas R S, Li J, McConville W, Cooley B J, Lund M S, Samarth N, Leighton C, Crespi V H and Schiffer P, Artificial spin ice in a geometrically frustrated lattice of nanoscale ferromagnetic islands, Nature **439** 303 (2006).

[8] Gliga S, Kákay A, Hertel R, and Heinonen O G, Spectral analysis of topological defects in an artificial spin-ice lattice, Phys. Rev. Lett. **110** 117205 (2013).

[9] Iacocca E, Gliga S, Stamps R L, and Heinonen O, Reconfigurable wave band structure of an artificial square ice, Phys. Rev. B **93** 134420 (2016).

[10] Jungfleisch M B *et al.*, Dynamic response of an artificial square spin ice, Phys. Rev. B **93** 100401(R) (2016).

[11] Lasnier T D and Wysin G M, Magnetic oscillation modes in square lattice artificial spin ice. Phys. Rev. B **101** 224428 (2020).

[12] Wysin G M, Metastability and dynamics in remanent states of square artificial spin ice with long-range dipole interactions, Phys. Rev. B **108** 174405 (2023).

[13] Heisenberg W, Zur Theorie des Ferromagnetismus, Z. Phys. **49** 619 (1928).

[14] Jiles D, *Introduction to Magnetism and Magnetic Materials* (London: Chapman and Hall 1991) Ch 11.

[15] Arroo D M, Gartside J C, and Branford W R, Sculpting the spin-wave response of artificial spin ice via microstate selection, Phys. Rev. B **100** 214425 (2019).

[16] Arora N and Das P, Spin wave spectral probing of degenerate microstates in building-block of square artificial spin ice, AIP Advances **11** 035030 (2021).

[17] Edberg R, Spin ice under uniaxial pressure and magnetic frustration in garnets *PhD dissertation* KTH Royal Institute of Technology, Nordforsk (2021) (http://urn.kb.se/resolve?urn=urn:nbn:se:kth:diva-293527).

[18] Wysin G M, Metastability and dynamic modes in magnetic island chains, J. Phys.: Condens. Matter **34** 065803 (2022).

[19] Wysin G M, Moura-Melo W A, Mól L A S and Pereira A R, Magnetic anisotropy of elongated thin ferromagnetic nano-islands for artificial spin ice arrays, J. Phys.: Condens. Matter **24** 296001 (2012).

[20] Wysin G M, Moura-Melo W A, Mól L A S and Pereira A R, Dynamics and hysteresis in square lattice artificial spin ice, New J. Phys. **15** 045029 (2013).

[21] Yue L and Liou S H, Magnetic Force Microscopy Studies of Magnetic Features and Nanostructures, in Bhushan B (ed) *Scanning Probe Microscopy in Nanoscience and Nanotechnology 2. NanoScience and Technology*, (Springer, Berlin, Heidelberg 2011). https://doi.org/10.1007/978-3-642-10497-8_10

[22] Haider T, A review of magneto-optic effects and its application, Int. J. Electromagn. Appl. **7** 17 (2017).

[23] Kimel A *et al.*, The 2022 magneto-optics roadmap, J. Phys. D: Appl. Phys. **55** 463003 (2022).

[24] Wittborn J, Rao K V, Proksch R, Revenko I, Dahlberg E D, and Bazylinski D A, Magnetization reversal observation and manipulation of chains of nanoscale magnetic particles using the magnetic force microscope, Nanostruct. Mater. **12** 1149 (1999).

[25] García J M, Thiaville A, Miltat J, Kirk K J, and Chapman J N, MFM imaging of patterned permalloy elements under an external applied field, J. Magn. Magn. Mater. **242–245** 1267 (2002).

[26] Tang H, Zhan X, Wu Z, Du Y, Talbi A, Pernod P, Controllable and facile fabrication of Fe nanoparticles/nanochains and their magnetic properties, J. Magn. Magn. Mater. **377** 472 (2015).

[27] Zhang Y *et al.*, Controlled synthesis of Co_2C nanochains using cobalt laurate as precursor: Structure, growth mechanism and magnetic properties, J. Magn. Magn. Mater. **456** 71 (2018).

[28] García J M, Thiaville A, Miltat J, MFM imaging of nanowires and elongated patterned elements, J. Magn. Magn. Mater. **249** 163 (2002).

[29] https://en.wikipedia.org/wiki/Clausen_function
[30] Anand M, Thermal and dipolar interaction effect on the relaxation in a linear chain of magnetic nanoparticles, J. Magn. Magn. Mater. **522** 167538 (2021).
[31] Bahiana M, Pereira Nunes J P, Altbir D, Vargas P, and Knobel M, Ordering effects of the dipolar interaction in lattices of small magnetic particles, J. Magn. Magn. Mater. **281** 372 (2004).